Journal of Computational Physics 229 (2010) 5299–5314

Contents lists available at ScienceDirect

Journal of Computational Physics

journal homepage: www.elsevier.com/locate/jcp

Coarse-grained computation for particle coagulation and sintering processes by linking Quadrature Method of Moments with Monte-Carlo

Yu Zou [a], Michail E. Kavousanakis [a], Ioannis G. Kevrekidis [a,b,*], Rodney O. Fox [c]

[a] Department of Chemical Engineering, Princeton University, Princeton, NJ 08544, USA
[b] Program in Applied and Computational Mathematics, Princeton University, Princeton, NJ 08544, USA
[c] Department of Chemical and Biological Engineering, Iowa State University, Ames, IA 50011, USA

ARTICLE INFO

Article history:
Received 8 August 2009
Received in revised form 21 December 2009
Accepted 2 March 2010
Available online 27 March 2010

Keywords:
Quadrature Method of Moments
Monte-Carlo simulation
Equation-free computation
Coagulation
Sintering

ABSTRACT

The study of particle coagulation and sintering processes is important in a variety of research studies ranging from cell fusion and dust motion to aerosol formation applications. These processes are traditionally simulated using either Monte-Carlo methods or integro-differential equations for particle number density functions. In this paper, we present a computational technique for cases where we believe that accurate closed evolution equations for a finite number of moments of the density function exist in principle, but are not explicitly available. The so-called equation-free computational framework is then employed to numerically obtain the solution of these unavailable closed moment equations by exploiting (through intelligent design of computational experiments) the corresponding fine-scale (here, Monte-Carlo) simulation. We illustrate the use of this method by accelerating the computation of evolving moments of uni- and bivariate particle coagulation and sintering through short simulation bursts of a constant-number Monte-Carlo scheme.

1. Introduction

Simulation of particle coagulation and sintering processes has been widely employed in chemical science and engineering to explore and understand particle formation phenomena such as colloidal aggregation, cell fusion and aerosol condensation. Models for such particle processes typically consider only one (volume) or two (volume and surface area) particle states (e.g. [1,2]). Particles aggregate, thus forming a new particle with larger volume; each particle may also experience restructuring, conserving its volume while reducing its surface area. Particle breakage may be also involved.

Conventional simulation techniques generally fall in two categories. The first one involves closed-equation descriptions for the evolution of particle distributions. Population Balance Equations (PBE) of particle number densities have long been used to describe the evolution of particle aggregation-breakage processes [3,4]. Except for some special situations, analytical solutions of these PBEs are not available. Numerical methods must be used to discretize and solve such equations, a typically computationally intensive task. Since normally only a finite number of low-order moments are of primary interest (e.g. for comparison with experiments) the Quadrature Method of Moments (QMOM) has been used in recent years to discretize and solve such moment equations [5–7]. The computational effort for solving QMOM descriptions is then dramatically reduced, compared to solving the full PBE, since the number of relevant degrees of freedom is reduced. A computational alternative to

* Corresponding author at: Department of Chemical Engineering, Engineering Quadrangle, Princeton University, Princeton, NJ 08544, USA. Tel.: +1 609 258 2818; fax: +1 609 258 0211.
E-mail addresses: yzou@Princeton.EDU (Y. Zou), mkavousa@Princeton.EDU (M.E. Kavousanakis), yannis@Princeton.EDU (I.G. Kevrekidis), rofox@iastate.edu (R.O. Fox).

0021-9991/$ - see front matter © 2010 Elsevier Inc. All rights reserved.
doi:10.1016/j.jcp.2010.03.007

QMOM is the Direct Quadrature Method of Moments (DQMOM) [8,9], which solves directly for the quadrature weights and abscissas involved in the moment approximation.

The other category of simulation techniques involves Monte-Carlo (MC) simulation. It further divides in two branches: constant-volume MC (CVMC) [10–12] and constant-number MC (CNMC) [2,13]. In both MC methods, an ensemble of particles is used to mimic the real evolution of the coagulation and/or sintering process. At some reporting time steps, coarse-grained quantities such as moments of volume (for the univariate case) or mixed moments of volume and surface area (for the bivariate case) are reported, obtained from the average of the ensemble of realizations. For the CVMC, every time a pair of particles is selected to aggregate, this coagulation event results in the net loss of one particle. For a total initial number N_0 of particles, the simulation process will terminate after $N_0 - 1$ coagulation steps. A drawback of this MC method is, therefore, the continuously decreasing accuracy due to the depletion of the particle array. In [2,13], a constant-number Monte-Carlo scheme was suggested as an alternative to CVMC. This method refills the particle array with one new particle at each coagulation step, thus retaining a constant number of particles. It was demonstrated that this scheme can efficiently reproduce analytical solutions [13] as well as QMOM-based computations of particle distribution moments [6].

In quadrature-based methods [7–9], once closed equations for moments or corresponding quadrature points are available, they can be solved efficiently using established ODE solvers. For cases in which such closed equations cannot be derived (e.g. when the fine-scale simulator is a molecular dynamics or a kinetic Monte-Carlo one for which no explicit kernel exists) we propose the application of the *Equation-Free* framework [14,16,17]; this framework enables fine-scale simulators to efficiently evolve coarse-grained observables, for which the corresponding macroscopic equations are not available in closed form. In this paper, we demonstrate how to circumvent the explicit derivation of such closed equations, and use instead a coarse-grained combination of the QMOM and MC simulation methods. We will "wrap" this computational approach around a CNMC fine-scale simulator in order to accelerate the computation of temporal evolution of aerosol coagulation and sintering. For these examples, explicit kernels do exist, and QMOM equations can be written down in closed form; we do not make use of these equations – instead we allow our equation-free procedure to solve them without writing them down. The efficiency of the proposed methodology is then compared to the direct simulation of the MC scheme and it is shown that the accuracy of the obtained moments is comparable to the results produced by direct MC simulations (and to those produced by the explicit QMOM equations). This subsequent comparison of the equation-free results with the explicit QMOM equation results validates the approach and shows evidence of (modest) acceleration – this was the reason for the illustrative example selection. We stress, however, that the real potential of the approach will be in cases where a physical simulator (e.g. a molecular dynamics one) is available but no accurate closed coagulation/sintering kernel is known.

The computational implementation involves the repeated generation of particle distributions consistent with few lower order moments, whose dynamics we are interested to accelerate. In this context we describe two different approaches for the generation of particle distributions (*lifting*): a δ-lifting and a maximum entropy (*maxent*) lifting. We demonstrate that, for the examples chosen, non-uniqueness of the generated particle distributions does not have an impact on the lower order moment evolution during the course of the computations. We reiterate that our algorithms can, in principle, be wrapped around *any* fine-scale simulator of the process, such as a molecular dynamics or a Brownian dynamics one.

The paper is organized as follows. In Section 2, we briefly review existing simulation methods for particle coagulation and sintering processes. Section 3 describes our equation-free framework, through which coarse-grained computations based on a fine-scale simulator can be performed; in our case, the fine-scale simulator is a CNMC one. Numerical results are presented and discussed in Section 4, followed by conclusions and a brief discussion in Section 5.

2. Existing simulation methods

2.1. Population Balance Equations

The continuous equation for the evolution of the number density of particles in terms of the particle volume, when only aggregation is considered, was first derived in [3]. It is given by:

$$\frac{\partial n(v,t)}{\partial t} = \frac{1}{2}\int_0^v \beta(v-v',v')n(v-v',t)n(v',t)\,\mathrm{d}v' - n(v,t)\int_0^\infty \beta(v,v')n(v',t)\,\mathrm{d}v', \tag{2.1}$$

where $n(v,t)$ is the number density of particles as a function of the particle volume and $\beta(v,v')$ is the coagulation kernel expressing the rate at which particles with volume v and v' combine to form a new particle with volume $v+v'$.

If particles also experience restructuring of their surface area after each coagulation event, Eq. (2.1) can be written in a bivariate form [18,6]:

$$\begin{aligned}\frac{\partial n(v,a,t)}{\partial t} = {} & \frac{1}{2}\int_0^v\int_0^a \beta(v-v',v',a-a',a')n(v-v',a-a',t)n(v',a',t)\,\mathrm{d}v'\,\mathrm{d}a' \\ & - n(v,a,t)\int_0^\infty\int_0^\infty \beta(v,v',a,a')n(v',a',t)\,\mathrm{d}v'\,\mathrm{d}a' - \frac{\partial}{\partial a}(\dot{a}n(v,a,t)),\end{aligned} \tag{2.2}$$

where $\dot{a}$ is the time rate of change of particle surface area due to sintering (restructuring). This rate is often modeled as a linear form [1]:

$$\dot{a} = -\frac{1}{t_f}(a - a_{min}), \tag{2.3}$$

where $a_{min} = \pi(6v/\pi)^{2/3}$ is the area of the fully compacted (spherical) particle and t_f is a characteristic time scale for particle sintering.

Modifications of the above equations involve adding terms related to fragmentation. Since this paper only deals with particle coagulation and sintering, we do not consider such additional terms; the interested reader may refer to [19] for further information. We reiterate, however, that including additional terms in the simulation does not alter the "wrapper" structure of our acceleration algorithms.

2.2. Quadrature Method of Moments

For the CNMC univariate case, the moments of the volume-based distribution function are defined as:

$$\mathcal{M}_k = \int_0^\infty v^k n(v)\,\mathrm{d}v. \tag{2.4}$$

If the integral on the right-hand side of the above equation is approximated by quadrature, i.e.:

$$\mathcal{M}_k = \int_0^\infty v^k n(v)\,\mathrm{d}v \approx \sum_{i=1}^{N} \omega_i v_i^k, \tag{2.5}$$

where ω_i and v_i are the corresponding weights and abscissas, then Eq. (2.1) can be approximated by coupled moment equations [5]:

$$\frac{\mathrm{d}\mathcal{M}_k}{\mathrm{d}t} = \frac{1}{2}\sum_{i=1}^{N}\sum_{j=1}^{N}\left[(v_i + v_j)^k - v_i^k - v_j^k\right]\beta(v_i, v_j, a_i, a_j)\omega_i\omega_j. \tag{2.6}$$

The computation of the quadrature weights and abscissas on the right-hand-side of the above equations can be done by building a sequence of polynomials orthogonal to the unknown distribution (for which the only available information consists of the values of a few of its lower order moments). The abscissas are the roots of the highest-order polynomial and the values of the weights arise as the solution of a linear system constructed from the values of the moments [20–22]. A robust computation of the quadrature points at each temporal integration step can be obtained through the Product Difference method [21,5,7]. The approximation of the quadrature points is determined by the solution of an eigenvalue problem, involving a real symmetric tridiagonal matrix [23] (see also the subroutines ORTHOG and ZRHQR in [22]). ORTHOG requires as input the modified moments of the distribution $n(v)$ given by:

$$v_k = \int_0^\infty \pi_j^k n(v)\,\mathrm{d}v, \tag{2.7}$$

where the polynomials π_j are generated by the recurrence relation:

$$\begin{aligned} &\pi_{-1}(v) \equiv 0,\\ &\pi_0(v) \equiv 1,\\ &\pi_{j+1}(v) = (v - \alpha_j)\pi_j(v) - \beta_j\pi_{j-1}(v), \quad j = 0, 1, 2, \ldots \end{aligned} \tag{2.8}$$

In our computations, we set $\alpha_j,\ \beta_j = 0$, so that the modified moments v_k are the moments of the distribution $n(v)$ given by (2.4).

In the bivariate situation, the distribution function is expressed over the volume v and surface a of particles. The moments of the bivariate distribution are defined as:

$$\mathcal{M}_{kl} = \int_0^\infty \int_0^\infty v^k a^l n(v, a)\,\mathrm{d}v\,\mathrm{d}a. \tag{2.9}$$

When expressing the mixed moments of volume and surface area in terms of a quadrature form, i.e.:

$$\mathcal{M}_{kl} = \sum_{i=1}^{N} v_i^k a_i^l \omega_i, \tag{2.10}$$

Eq. (2.2) reads [6]:

$$\frac{\mathrm{d}\mathcal{M}_{kl}}{\mathrm{d}t} = \frac{1}{2}\sum_{i=1}^{N}\sum_{j=1}^{N}\left[(v_i + v_j)^k(a_i + a_j)^l - v_i^k a_i^l - v_j^k a_j^l\right]\beta(v_i, v_j, a_i, a_j)\omega_i\omega_j + l\sum_{i=1}^{N} v_i^k a_i^{l-1}\dot{a}|_{a=a_i}\omega_i, \tag{2.11}$$

where N is the number of quadrature weights and abscissas.

Fractional, rather than integral, moments are frequently chosen to improve the numerics (to avoid placing too much emphasis on the tail of distribution) [6]. The Product Difference algorithm is applicable to the univariate case. For the bivariate case, quadrature points – given the values of mixed moments – are obtained by solving to zero (using the conjugate gradient method) a minimization problem [6]. For the case of a 36 fractional moment expansion, including all moments of order $\frac{k}{3}$, $\frac{l}{3}$ with $k,\ l = 0,\ldots,5$ using 12-point quadrature $((a_i, v_i, w_i),\ i = 1,\ldots,12)$, the corresponding objective function is:

$$J(v_i, a_i, w_i) = \sum_{k=0}^{5}\sum_{l=0}^{5}\left[\frac{\sum_{i=1}^{N} v_i^{k/3} a_i^{l/3}\omega_i - \mathcal{M}_{k/3,l/3}}{\mathcal{M}_{k/3,l/3}}\right]^2. \tag{2.12}$$

2.3. Constant-number Monte-Carlo simulation

Direct, long-time Monte-Carlo simulations can be performed in order to obtain the moment dynamics of coagulation/sintering processes. Since the computational requirements for an efficient study of MC simulations are very high, we resort to alternative techniques, such as the equation-free framework [14,16,17], which wraps around the particle-based simulator and can enable the acceleration of temporal computations. The computational advantages of the equation-free method should be compared to full simulations using particle-based (Monte-Carlo, or possibly molecular dynamics) simulators. We will focus only on constant-number Monte-Carlo simulation in this paper, and illustrate our coarse-graining approach by accelerating its time-marching.

In CNMC a random pair of particles, (i,j), and a random real number p with uniform distribution are chosen. A coagulation event takes place whenever $p < \beta(v_i, v_j)/\beta_{max}$, where β_{max} is the largest coagulation rate amongst all pairs of particles. Volumes and surface areas of the two coagulating particles are added and assigned to one of the particles. The vacancy is then filled with a particle randomly chosen from the particle array. The inter-event time increment is computed as [13]:

$$\Delta t_\kappa = \frac{2V_0}{N_p\langle\beta_{ij}\rangle}\frac{1}{N_p}\left(\frac{N_p}{N_p-1}\right)^\kappa, \tag{2.13}$$

where V_0 is the initial total volume of all particles, N_p the constant number of particles, κ the index of the coagulation event, and $\langle\beta_{ij}\rangle$ is the average value of coagulation rates over all particle pairs. It can be seen that V_0/N_p is simply the first-order moment of volume M_1. If sintering is also considered, we need to integrate (2.3) over each such time step.

3. Coarse-grained QMOM–MC computation

The equation-free framework [14,16,17] for modeling and computation of complex/multiscale systems gives rise to a class of algorithms that combine short bursts of fine-scale simulation with traditional continuum numerical methods. Linking between different levels of modeling involves a coarse time stepper: starting from initial values of coarse-grained-level observables (here, moments) of a fine-scale system, we *lift* these values to generate an ensemble of consistent fine-level states (e.g. particle distributions). These fine-level states are then evolved forward in time through an *inner simulation* (here CNMC). A short time later the coarse-grained observables (moments) are computed again from the fine states (from the new particle distributions); this is the *restriction* step. This short-time evolution of moments, observed through the coarse time stepper, can be used to estimate their temporal derivatives, which can then be incorporated into an *outer* numerical integration scheme (e.g. forward Euler, Runge–Kutta, etc.) to accelerate the numerical evolution of the coarse observables (moments). If a separation of time scales exists between different levels of system description (i.e., if the evolution of the moments is significantly slower than individual particle coagulation/sintering events) the time step for this *outer* integration can be chosen relatively large, so that the overall computational time is significantly less than that of full discrete event simulation. In effect, we are integrating the (unavailable) moment equations using the outer integrator scheme; yet the necessary values of the time derivatives of the moments (e.g. if we were studying a constant volume model, the right-hand-sides of (2.6) and (2.11)) are not obtained through function evaluations, but rather through short bursts of computational experiments with the fine-scale CNMC code.

Since only a finite number of particles are generated in the discrete CNMC, an ensemble of replica copies of particle pools must be averaged for reducing statistical noise. Note that, if accurate closed equations in terms of a finite number of moments exist, the evolution of these coarse observables should be, in principle, insensitive to particular realizations of *lifting*; we will return to this issue while discussing our computational results below.

In this paper *Coarse Projective Integration* [24–26], – a particular equation-free technique – is employed, which aims at decreasing the total CNMC computational time required for studying the dynamics of coagulation and sintering processes. The implementation of the discrete event simulation was described in Section 2.3; equation-free computation employs two steps that link this fine-scale simulator with coarse-level computation: *restriction* and *lifting*. The *restriction* step (computing moments of a particle distribution) is trivial: if N_p particles are employed at each simulation and particle m has volume v_m and area a_m then, e.g. for the bivariate case, the mixed moment M_{kl} is evaluated from:

$$M_{kl} = \left\langle \frac{1}{N_p} \sum_{m=1}^{N_p} v_m^k a_m^l \right\rangle, \tag{3.1}$$

where $\langle\ \rangle$ denotes the average over several replica copies of the stochastic simulation.

The *lifting* step (realizing particle distributions consistent with a number of prescribed moment values) is implemented in two stages:

- Compute quadrature abscissas and weights corresponding to particular moments of the particle distribution. Moment inversion algorithms based on Wheeler's approach [27], using the subroutines ORTHOG and ZRHQR in [22] were employed in this paper to perform the computation of the quadrature abscissas and weights for the univariate case. In the bivariate case, the inversion of the mixed moments M_{kl}, involves the minimization of (2.12). At the beginning of the simulation, for a δ-function initial distribution, we used equally-weighted coincident points. During the coarse-grained computation process, the quadrature points from the previous outer integration step can serve as the initial condition for the next minimization. Details for the application of the minimization process can be found in [6].
- Generate δ-function distributed particles from quadrature abscissas and weights (lifting). For instance, suppose a 12-point quadrature $((v_i, a_i, w_i),\ i = 1, 2, \ldots, 12)$ is used for the bivariate case. A random variable p with a uniform distribution $U(0, 1)$ is first generated; then the particle is assigned volume and area (v_k, a_k) if $\sum_{i=1}^{k-1} w_i < p < \sum_{i=1}^{k} w_i$. This process is repeated until all N_p particles are assigned values of volume and area (this procedure also applies to the univariate case).

An alternative approach to generating consistent microscopic realizations with a small number of moment values is based on the Maximum Entropy (*maxent*) method (see, e.g. [28,29]). Details of the approach are briefly reported in the Appendix; this generates a smoother approximate realization of the particle number density function, as compared to the δ-function based lifting. We observed that, for our illustrative example, the two lifting approaches gave essentially identical coarse results; this will be further discussed in Section 4.

4. Numerical results

In this section, we present coarse-grained simulations for two cases: a coagulation example, where the coarse variables are univariate distribution moments (Section 4.2), and a coagulation-sintering example, where the coarse variables are bivariate distribution moments (Section 4.3). Before production runs are carried out, however, it is important to test whether the chosen finite number of moments in each case are sufficient to accurately describe the problem. In other words, we want to test whether closed equations in terms of these chosen variables exist, even though we cannot explicitly derive them.

4.1. Testing the level of closure for univariate QMOM–MC

If the number of governing moments (that is, the level at which the moment equations close) has been chosen correctly, the effect of initializing higher moments (moments of order higher than those chosen) in various different ways, should get quickly forgotten as the simulation progresses. In other words, higher-order moments become quickly "slaved" to the governing ones (a phenomenon associated with separation of time scales, which is sometimes referred to as "healing" [15,16]). This is practically tested by starting with a set of initial values of the lower (slow, governing) moments, and constructing several distributions (performing several liftings) consistent with them; each such lifting has different values for the higher-order moments. The test consists of examining whether the lower (slow, governing) moment values at the end of a relatively short fine-scale simulation are indeed insensitive to the details of the lifting procedure (alternatively, to the initialization of the higher-order moments).

In these simulations a Brownian coagulation kernel is used [30,6]:

$$\beta(u, v) = K(u^{1/D_f} + v^{1/D_f})(u^{-1/D_f} + v^{-1/D_f}). \tag{4.1}$$

Throughout this work, the values of the coefficients in the above kernel are taken as $K = 1$ and $D_f = 3$. We choose six low moments as our coarse variables, and set their initial values to $M_{i/3} = 1,\ i = 0, 1, \ldots, 5$, corresponding to a three-point quadrature $v_1 = 1,\ w_1 = 1;\ v_2 = 0,\ w_2 = 0;\ v_3 = 0,\ w_3 = 0$. An ensemble of $N_p = 10,000$ particles are generated according to this initial condition and evolved through $t = 0.3$ by using the CNMC algorithm. Fractional moments are reported at successive steps $t = k\,\mathrm{d}t,\ k = 0, 1, \ldots, 300$, where $\mathrm{d}t = 0.001$. For the purpose of noise reduction, 100 replica copies of particles ensembles are averaged to estimate accurate values of fractional moments. The evolution is paused at time $t = 0.1$ and the values of the six leading moments are reported, and used to construct a three-point quadrature, i.e. to calculate the corresponding quadrature abscissas and weights.

We now proceed to our test. On the one hand, we continue the paused CNMC simulation in the time interval [0.1, 0.3] and report the "naturally evolved" values of the governing moments. On the other hand, we construct a realization of particles with a volume distribution consisting of three δ-functions, corresponding to the reported quadrature at $t = 0.1$, and subsequently evolve this new distribution using the same coagulation dynamics. Fig. 1(a) shows trajectories of the six moments during this test. Relative errors between the naturally evolved simulation (the "true" moments, $M_{i/3}^{true},\ i = 0, 1, \ldots, 5$), and

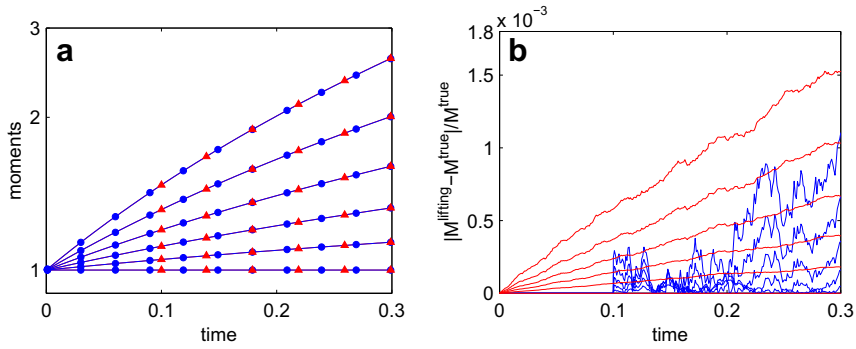

Fig. 1. (a) Evolution of six moments as obtained from direct CNMC ("true" moments) and moments after δ-lifting at $t = 0.1$ by using three quadrature points. Blue lines with circles: six "true" moments, $M_{i/3},\ i = 0, 1, \ldots, 5$; red lines with triangles: six moments after δ-lifting (they visually coincide). (b) Relative errors between six "true" moments and moments after δ-lifting using three quadrature points. Blue lines: relative errors of moments; red lines: $2\sigma_M/M^{true}$, where σ_M is the standard deviation of the noise in the moments estimated using 100 replica copies. (For interpretation of the references in color in this figure legend, the reader is referred to the web version of this article.)

those obtained after the δ-lifting, $M_{i/3}^{lifting},\ i = 0, 1, \ldots, 5$, remain within 0.15% (Fig. 1(b)) in the time interval [0.1,0.3]. These deviations are within the order of magnitude of the quantities $2\sigma_M/M^{true}$, where σ_M is the standard deviation of the moments M computed by using 100 direct CNMC replicas. This interval encompasses 96% of our realizations. This evidence strongly supports our hypothesis of the existence of an accurate six-moment closure.

In addition to the moments themselves, the evolution of the time derivatives of the moments with and without δ-lifting are compared as well (Fig. 2(a)). Since the observed variation in the moment values across replicas is of the order of 10^{-3}, a relatively large time duration $h = 0.02$ is used to estimate the temporal derivatives of moment evolution. The temporal derivatives are estimated through a linear least-square fitting by using $h/\mathrm{d}t(= 20)$ moment values at equally spaced time points with step dt. Relative errors of these derivatives are also shown to be of the order of the magnitude of the noise (Fig. 2(b)).

The above results suggest that the evolution of the six moments *and their temporal derivatives* can be well approximated by short bursts of CNMC coagulation dynamics consistently initiated through a δ-lifting. This suggests that, over the time scales we simulate, a closed description based on six fractional moments may indeed provide an accurate description.

What happens to the values of the higher-order moments, which were initialized differently? When the moments $(M_{i/3},\ i = 6, 7, \ldots, 19)$ are considered, we can see from Fig. 3(a) that their values will quickly approach their "true" ("natural") evolution values within a time interval of $\Delta t = 0.1$. Fig. 3(b) displays the relative errors in their values, indicating that these relative errors quickly become small compared to stochastic fluctuations. This corroborates our previous deduction: it is, indeed, reasonable to believe that the evolution of the 20 moments, $M_{i/3},\ i = 0, 1, 2, \ldots, 19$, can be well reproduced by δ-lifting using only six moments, $M_{i/3},\ i = 0, 1, \ldots, 5$. In other words, it appears that the higher-order moments become relatively quickly slaved to the lower order ones; δ-lifting based on only six moments or a three-point quadrature appears adequate for equation-free acceleration of the computation here.

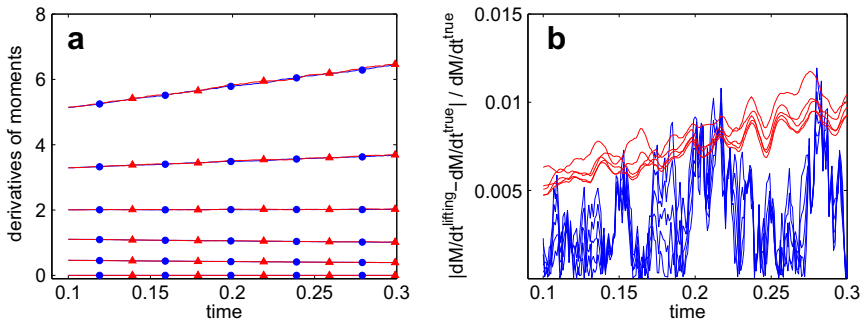

Fig. 2. (a) Approximation of temporal derivatives of six moments from direct CNMC ("true" moments) and moments after δ-lifting at $t = 0.1$ by using three quadrature points. The time duration for the approximation of the derivatives is $h = 0.02$. Blue lines with circles: temporal derivatives of six "true" moments; red lines with triangles: temporal derivatives of moments after δ-lifting. (b) Relative errors between derivatives of six "true" moments and of moments after δ-lifting by using three quadrature points. Blue lines: relative errors; red lines: $\frac{2\sigma_{\mathrm{d}M/\mathrm{d}t}}{\mathrm{d}M/\mathrm{d}t^{true}}$, where $\sigma_{\mathrm{d}M/\mathrm{d}t}$ is the standard deviation of the temporal derivatives of the moments obtained across 100 replica copies. (For interpretation of the references in color in this figure legend, the reader is referred to the web version of this article.)

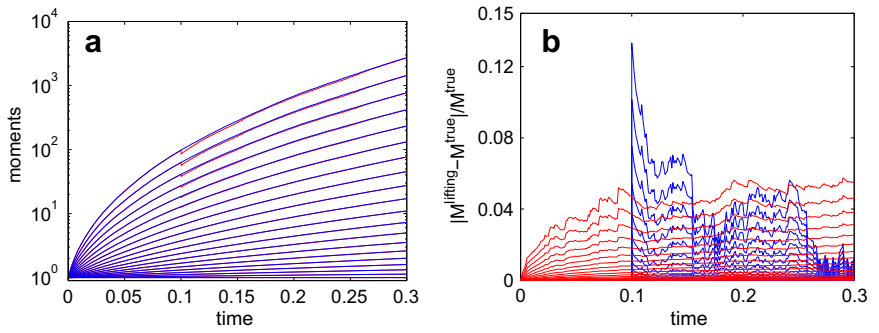

Fig. 3. (a) Evolution of 20 moments from direct CNMC ("true" moments) and moments after δ-lifting at $t = 0.1$ by using three quadrature points. Blue lines: 20 "true" moments, $M_{i/3},\ i = 0, 1, \ldots, 19$; red lines: 20 moments after δ-lifting. (b) Relative errors between 20 "true" moments and moments after δ-lifting by using three quadrature points. Blue lines: relative errors of moments; red lines: $2\sigma_M/M^{true}$, where σ_M is the standard deviation of the moments obtained across 100 replica copies. (For interpretation of the references in color in this figure legend, the reader is referred to the web version of this article.)

Having confirmed that six moments are adequate for an accurate closure, it is also natural to ask whether a smaller number of moments may suffice. To explore the possibility of using even fewer quadrature points to form a successful closure for moment equations, we tried respectively employing two quadrature points to represent the four lowest-order moments and one quadrature point for the two lowest-order moments at time $t = 0.1$. Similarly to the case of three quadrature points, the particle dynamics is initiated with distributions corresponding to δ-liftings based on these reduced quadrature representations. The evolution of the relative error in the values of the six lowest-order moments are reported again in Fig. 4. It can be concluded from these figures that the 4(2) lowest-order moments can be closed with 2(1) quadrature points. However, higher-order moments are not well represented (see Fig. 5) in these two cases. Although there is still a trend for these higher-order moments to return to their true trajectories, this return ("healing") takes place quite slowly compared to the three-points case. Therefore, as far as the higher-order moments (up to $M_{19/3}$) are concerned, one- or two-point representations are not good options for implementing the δ-lifting procedure and the three-point quadrature (or six lower moments representation) has to be used.

Before we proceed to the actual results, two more points are worth addressing briefly. The first concerns the nature of the kernel in (4.1). Notice that the coagulation rate resulting from this particular kernel does not depend on sintering; this is, of course, an approximation, since $D_f = 3$ suggests that the coagulating particles have spherical shape. More complicated coagulation kernels can be found in the literature (e.g. see [18]). These kernels account for the effect of sintering by allowing the fractal dimension of an aggregate to depend on its surface area, which slightly modifies the effective collision radius. It is important to note that these modifications do not affect in a significant way the mathematical form of the coagulation kernel, and thus we will use the simpler kernel above to illustrate our computational methodology. Nonetheless, we reiterate that our approach is not limited by the particular features of specific kernels and that it is especially designed for cases where closed expressions (e.g. explicit kernels) for the coagulation rate are not available.

The second point concerns the selection of the appropriate h value for the time-derivative estimation as illustrated in Fig. 6. As the value of h is reduced, the effect of noise becomes significant, so that detrimental fluctuations in the derivative estimates may arise. The value of h cannot be very long either, since then linear fitting will lead to overly smoothened estimates of the time derivatives. In Fig. 6, we depict the dependence of the estimated time derivative values, $\frac{dM_{5/3}^{true}}{dt}$, on

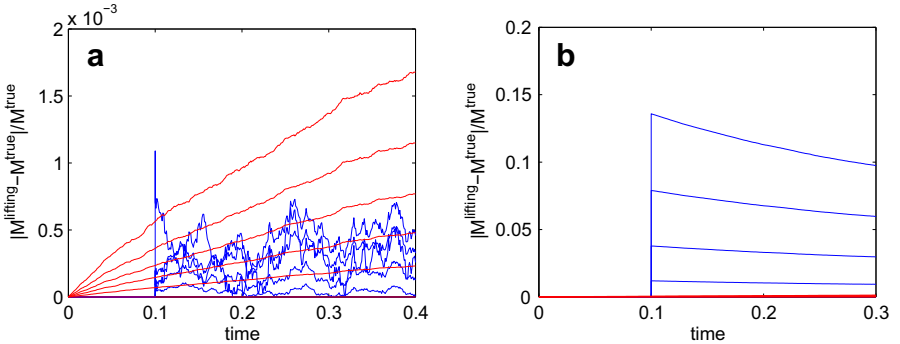

Fig. 4. Relative errors between six "true" moments $M_{i/3},\ i = 0, 1, \ldots, 5$ and moments after δ-lifting at time $t = 0.1$ by using (a) two quadrature points and (b) one quadrature point. Blue lines: relative errors of moments; red lines: $2\sigma_M/M^{true}$, where σ_M is the standard deviation of the moments obtained across 100 replica copies. (For interpretation of the references in color in this figure legend, the reader is referred to the web version of this article.)

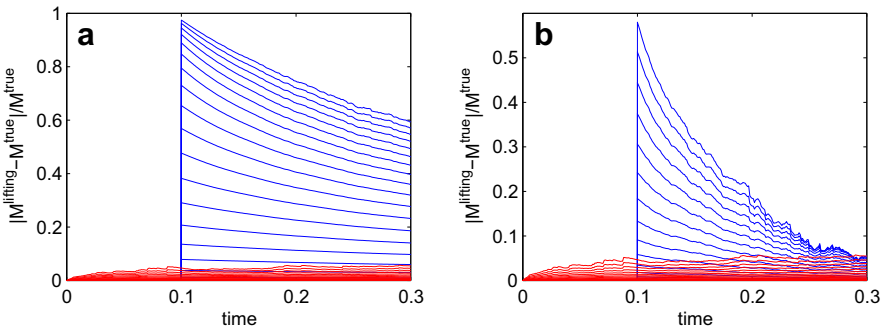

Fig. 5. Relative errors between 20 "true" moments and moments after δ-lifting at time $t = 0.1$ by using (a) one and (b) two quadrature points. Blue lines: relative errors of moments; red lines: $2\sigma_M/M^{true}$, where σ_M is the standard deviation of the moments obtained by taking 100 replica copies. (For interpretation of the references in color in this figure legend, the reader is referred to the web version of this article.)

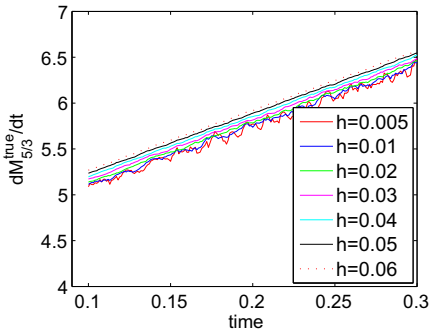

Fig. 6. Temporal derivatives of $(M_{5/3})$ moment estimated using different values of the time step size h. (For interpretation of the references in color in this figure legend, the reader is referred to the web version of this article.)

the selection of the time step size h, where $M^{true}_{5/3}$ values are obtained from direct CNMC simulation. The appropriate h should then be (a) not too long, in order to preserve accuracy in our computations and (b) not too short, in order to filter excessive noise effects from the CNMC simulations. In this work, h was chosen in the range from 0.02 to 0.05. Other numerical approaches (e.g. Richardson extrapolation [31] or maximum likelihood estimation techniques [32]) may be used to estimate the moment temporal derivatives as well.

4.2. Coarse-grained simulation for univariate QMOM–MC

For the coarse-grained computation, 15 replica copies of $N_p = 10,000$ particles are used. Starting from the same initial condition as above, fractional moments of volume are obtained through restriction at times $t = 0.01k,\ k = 1, 2, \ldots, 10$. The moments, $M_{i/3},\ i = 0, 1, \ldots, 5$ at the last successive five steps are used to estimate the temporal derivatives $dM_{i/3}/dt$ through least-squares fitting. The temporal derivative estimates are passed to a forward Euler scheme to extrapolate moment evolution from $t = 0.1$ over a large time interval Δt_e (e.g. $\Delta t_e = 0.1, 0.2, 0.4$). Then the lift-evolve-restrict-project procedure is repeated. This procedure is schematically depicted in Fig. 7.

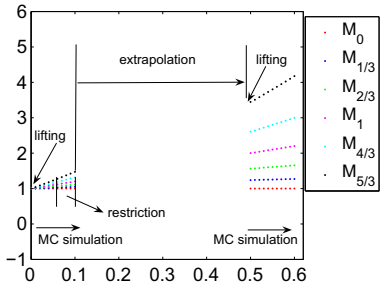

Fig. 7. Schematic illustration of coarse projective integration for the univariate QMOM–MC computations. (For interpretation of the references in color in this figure legend, the reader is referred to the web version of this article.)

As the projection interval Δt_e varies, the accuracy and the overall computational time for the moment evolution also vary. Fig. 8 reveals this trend: as Δt_e decreases, the accuracy of the projective integration improves. The moment evolution approximates increasingly well that of the CNMC; this, however, is obtained at the cost of increasing CPU time (see Fig. 9).

The dimensionless scaled univariate moments, defined by:

$$\mu_{k/3} = \frac{M_{k/3}}{M_0}\left(\frac{M_0}{M_1}\right)^{k/3}, \quad k = 0, 1, \ldots, 5, \tag{4.2}$$

are computed from this projective integration procedure and compared with those given by standard QMOM (Fig. 10). We see a trend of gradual approaching of the projective integration results to standard QMOM results as the projection step Δt_e is reduced.

4.2.1. Some observations on the effect of lifting

The lifting process with δ (Dirac) functions does not appear to influence the subsequent moment evolution, even though the lifted (reconstructed) distributions are significantly different from the corresponding naturally evolved distributions. In Fig.11(a), we depict snapshots of the particle distribution with respect to their volume, obtained from the univariate CNMC

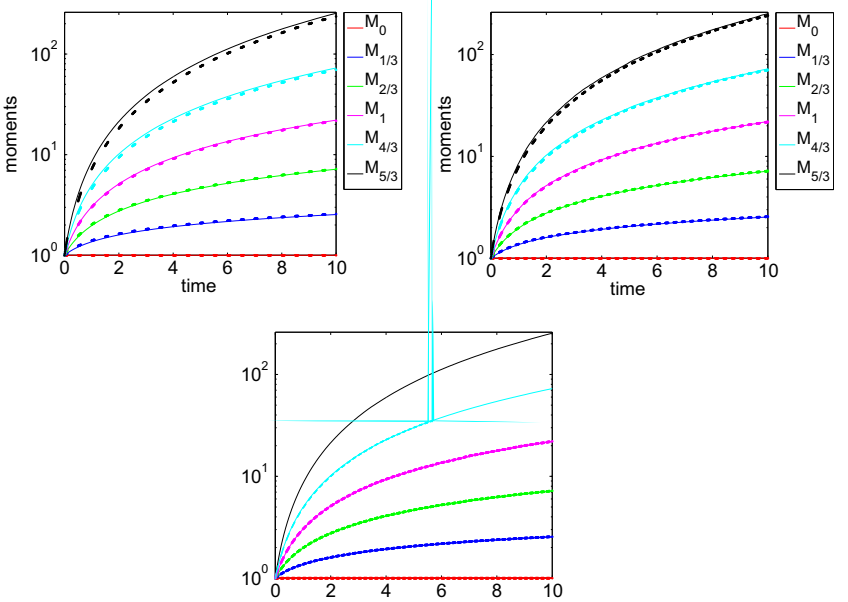

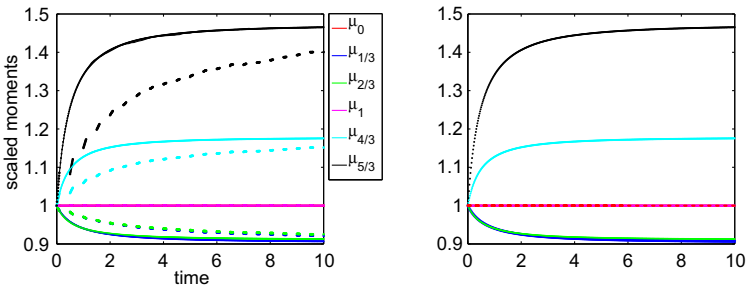

simulation over the time interval, $t \in [2,3]$ (Fig.11(b) depicts the respective smooth maxent representation). The initial condition is the same with the one used in Section 4.1. The simulation is interrupted at time $t = 3$ and two different lifting implementations are applied. The first considers δ-function distributed particles (see Section 3); the second lifting scheme is based on the maximum entropy approach, which is described in the Appendix.

This latter approach produces a smoother realization of the particle distribution, as compared to the direct simulation. In Fig.11(c), the cumulative distribution function of the particles with respect to their volume is compared to the distributions obtained after lifting with each of the two approaches (Dirac and maximum entropy (*maxent*)), based on the knowledge of six moments: $M_{i/3},\ i = 0,1,\ldots,5$. The Dirac lifting approximation produces a step-wise distribution, which does not quickly converge to the "real" distribution evolution (i.e., the one computed from direct simulation), even after a substantial period of time has elapsed (see Fig.11(d)). The *maxent* lifting produces a smooth approximation of the real distribution and, as time elapses, one can observe the tendency for convergence of the two distributions (they both approach a final, self-similar one).

Despite the fact that Dirac δ-lifting does not capture the real distribution well, it appears successful in reproducing the evolution of the lower moments. In Fig. 12, we depict the evolution of the moments $M_{2/3},\ M_{4/3}$ and $M_{5/3}$, as obtained from direct simulation, as well as simulations from Dirac or *maxent* lifting which has occurred at time $t = 3$. There is good agreement in the values of the moments, even in the case of Dirac lifting.

Moreover, in order to illustrate the accuracy of computations, we compare the results of the coarse-grained approach wrapped around the CNMC simulator, with results presented in [33,34]. In particular, we compare a few of the lower order moments and the geometric standard deviation obtained at a large time (e.g. $t = 32$), where the distribution has reached its self-preserving shape with the corresponding values of the self-preserving distribution in the continuum regime as presented in [33,34]. The comparison is performed for both lifting methods (δ and maxent lifting) (see Tables 1 and 2). In [33], a discrete-sectional model is employed for the calculation of the self-preserving distribution, where small particles are treated as discrete entities and the larger ones are grouped into sections. The section boundaries are defined according to:

$$v_k = f_s v_{k-1}, \tag{4.3}$$

where f_s is the section spacing factor (ranging from 1.08 to 3.0) and $v_{k-1},\ v_k$ are the lower and upper boundaries of each section. When the sectional model conserves numerically the square of the particle volume we refer to the v^2-models, while when the particle volume is conserved then the models are referred to as v-models (or mass conserving). In Table 2, we compare the geometric standard deviation as obtained from the coarse-grained approach (using either Dirac or maxent lifting) with corresponding values as obtained from different section spacings f_s and different models (v^2 or v-models).

4.3. Coarse-grained simulation for bivariate QMOM–MC

In the bivariate case, coagulation and sintering are both considered and each particle is characterized by its volume and its surface area. We use 36 mixed moments as our coarse observables with a 12-point quadrature to carry out the

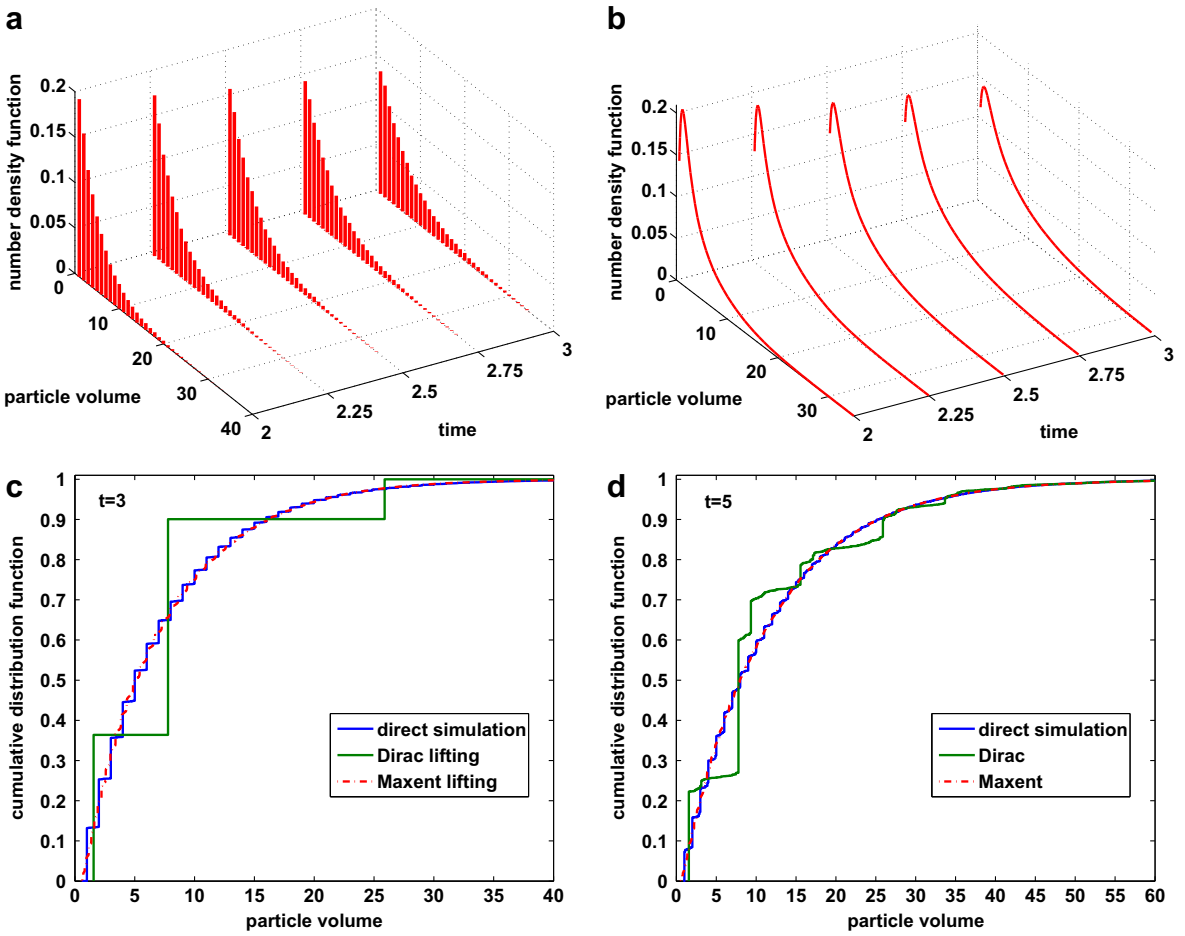

Fig. 11. (a) Snapshots of the univariate particle distribution evolution during the time interval $t \in [2, 3]$ and (b) the corresponding *maxent* distributions that share the same leading moment values. (c) Comparison of cumulative distribution functions, with respect to particle volume, for distribution functions sharing the same leading moment values. The blue line corresponds to the particle distribution obtained from direct CNMC at time, $t = 3$. The result of a consistent Dirac lifting, that retains the leading moment values, is depicted with the green line; the *maxent* distribution is depicted with red broken line. (d) Comparison of cumulative distribution functions at time, $t = 5$. The direct simulation distribution is depicted with blue line, the distribution evolved from the consistent Dirac lifting at $t = 3$ is the green line, and the distribution evolved from the consistent *maxent* lifting is the red broken line. (For interpretation of the references in color in this figure legend, the reader is referred to the web version of this article.)

computation. The initial condition in the bivariate QMOM–MC computation was chosen to be $M_{k/3,l/3} = 25.8^{l/3}$, with $k,\ l = 0, 1, \ldots, 5$. This corresponds to a 12-point quadrature: $(v_i, a_i, w_i) = (1, 25.8, 1),\ i = 1, \ldots, 12$. The Brownian kernel in (4.1) is again used. The characteristic time scale t_f in the sintering process is set to $t_f = 10$.

To avoid negative values of quadrature abscissas and weights, we replace $v_i,\ a_i,\ w_i$ in Eq. (2.12) with $v_i'^2,\ a_i'^2,\ w_i'^2$, respectively. Once optimized $v_i',\ a_i',\ w_i'$ are obtained, corresponding nonnegative values of $v_i,\ a_i,\ w_i$ are immediately available.

Similarly to the univariate case, immediately after the lifting, a short burst of simulation for bivariate dynamics is performed over a time interval of 0.1. Then, the mixed moments $M_{k/3,l/3},\ k,\ l = 0, 1, \ldots, 5$ obtained (through restriction) at $0.01i,\ i = 6, 7, \ldots, 10$ are used to estimate the corresponding temporal derivatives. These derivative values are subsequently passed to a forward Euler outer integration scheme to project the moment evolution over a "large" time step Δt_e.

Fig. 13(a) shows the time history of the projective integration results compared with those obtained by direct CNMC simulation. Good agreement is observed; a projective time step $\Delta t = 0.1$ results in a more faithful approximation of the dynamics compared to a step of $\Delta t = 0.2$. Fig. 13(b) compares the evolution of the dimensionless scaled moments defined by:

$$\mu_{k/3,l/3} = \left(\frac{M_{k/3,l/3}}{M_{0,0}}\right)\left(\frac{M_{0,0}}{M_{1,0}}\right)^{k/3}\left(\frac{M_{0,0}}{M_{0,1}}\right)^{l/3} \tag{4.4}$$

as obtained by our acceleration technique with full CNMC simulation as well as with bivariate QMOM simulation. Although time histories of actual moments given by the projective integration agree well with those of the direct CNMC simulation, the *dimensionless scaled* moments calculated from the projective integration results were seen to deviate more from those

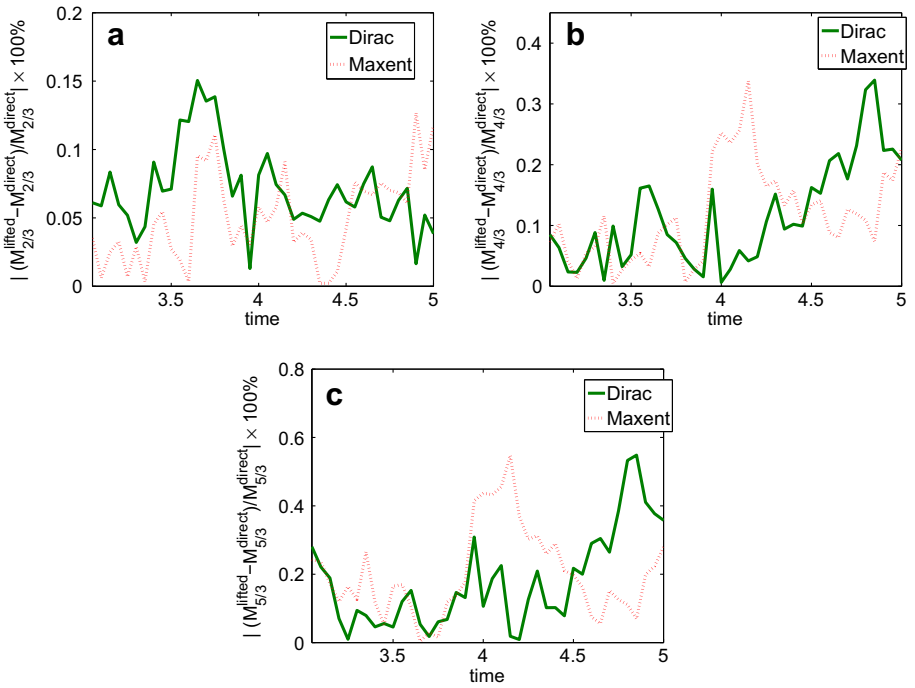

Fig. 12. Comparison of the evolution of moments, for the case of Dirac (green line) and *maxent* (red broken line) lifting at time $t = 3$, with the evolution of direct simulation moments. Figures (a)–(c) show the relative difference of the 2/3, 4/3 and 5/3th moments, M^{lift} after lifting occurs at $t = 3$ (through Dirac and *maxent*), from the corresponding "true" moments, M^{direct}, obtained through direct simulation. (For interpretation of the references in color in this figure legend, the reader is referred to the web version of this article.)

Table 1
Moments μ_i of the self-preserving distribution in the continuum regime as given by the QMOM–MC approach with different liftings and as found in the literature. The values in parentheses correspond to the relative % difference with the moments computed in Vemury et al. [33].

i	QMOM–MC		Vemury et al. [33]	Friedlander and Wang [34]
	Dirac	Maxent		
−1/2	1.5106 (−0.49%)	1.4868 (−2.06%)	1.5181	1.4476
−1/3	1.2637 (−0.28%)	1.2580 (−0.73%)	1.2673	1.2393
−1/6	1.1031 (−0.13%)	1.1024 (−0.20%)	1.1046	1.0843
0	1.0000 (−0.03%)	1.0000 (−0.03%)	1.0003	0.9847
1/6	0.9375 (+0.02%)	0.9371 (−0.02%)	0.9373	0.9242
1/3	0.9054 (+0.06%)	0.9047 (0.02%)	0.9049	0.8928
1/2	0.8979 (+0.07%)	0.8972 (−0.01%)	0.8973	0.8847
2/3	0.9118 (+0.07%)	0.9112 (0.00%)	0.9112	0.8967
5/6	0.9458 (+0.07%)	0.9454 (+0.03%)	0.9451	0.9274
1	1.0000 (+0.06%)	1.0000 (+0.06%)	0.9994	0.9765
2	1.9241 (+0.03%)	1.9322 (+0.46%)	1.9234	1.7788

Table 2
Geometric standard deviation of the self-preserving distribution in the continuum regime calculated by the QMOM–MC approach and models of [34,33].

Friedlander and Wang [34]	1.44
Vemury et al. [33]	
v^2-based model	
$f_s = 1.08$	1.445
$f_s = 1.5$	1.439
$f_s = 2.0$	1.426
v-based model	
$f_s = 1.08$	1.446
$f_s = 1.5$	1.462
$f_s = 2.0$	1.488
QMOM–MC	
Maxent	1.442
Dirac	1.435

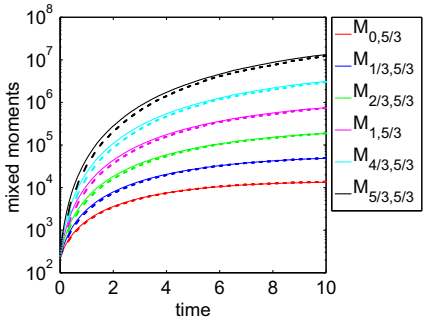

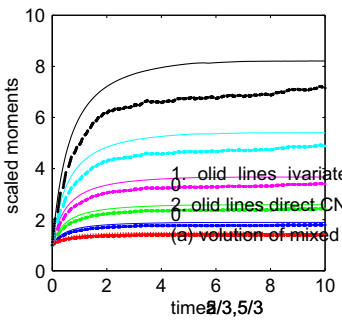

1. olid lines ivariate MM. Crossed lines direct CNMC. Dashe
0
2. olid lines direct CNMC. Dashed lines coarsegrained computation
6
(a) volution of mixed moments otained from the ivariate coarsegrai

obtained from the direct simulation. This disagreement may be at least partly attributed to the powers in (4.4) – a small discrepancy in the real moments will be magnified by these powers and cause a significant difference in the dimensionless scaled moment values. Overall, our equation-free QMOM–MC approach was clearly able to accelerate the direct CNMC simulation. In these illustrative examples, chosen with an eye towards validation, the acceleration was relatively modest (factors of 2–5); we reiterate that we expect the approach to be valuable when explicit kernels are not available (e.g. for molecular dynamics fine-scale simulators).

5. Conclusions

In this paper we focused on the development and implementation of a computational framework which aims at the acceleration of temporal computations for particle coagulation and sintering processes. We exploited this framework to accelerate constant-number Monte-Carlo simulations, using moments of the evolving distributions as coarse-grained variables. In effect, we solved QMOM evolution equations without actually writing them down in closed form. Bypassing the explicit derivation of closed moment equations we accelerated the computational exploration of long time behavior study through the application of Coarse Projective Integration. The simplest implementation of CPI was used here: projective Forward Euler. We note, however, that coarse integrators based on other traditional continuum integrator templates, such as coarse Adams–Bashforth, and even coarse *implicit* integrators for the case of stiff coarse equations can be formulated [24,25,15]. A finite number of volume moments for the univariate case and volume-surface area mixed moments for the bivariate case were our coarse-grained variables (observables). For the univariate case, we demonstrated that an implementation based on six low-order fractional moments was sufficient to describe the dynamics of the coagulation process; in the bivariate case we used 36 mixed moments in our coarse-grained computations. We then proceeded to quantify computational savings due to the application of the coarse projective scheme, while maintaining computational accuracy. We also showed how the accuracy of the projection step constrains the computational savings.

The equation-free approach significantly relies on the generation of particle states consistent with a given coarse-grained description (the *lifting* step). We implemented a δ-lifting, in which the distribution of particles is approximated by Dirac spikes. For our particular examples, we observed that even though this δ-lifting procedure does not accurately reproduce the "actual" particle distribution, the temporal evolution of the coarse variables (moments) appears to be captured remarkably well; while this is consistent with fast slaving of the higher-order moments, it may also imply that the higher-order moments provide relatively small perturbations to the evolution of the leading ones. For the univariate case we also described briefly a different lifting implementation, based on maximum entropy considerations, which generally gave rise to smoother lifted distributions, and which was also successful in capturing the moments evolution. While in our examples lifting was not a particularly time-consuming computational step, it is worth noting that in other applications of equation-free computation this could be the computational bottleneck that determines practical success of the approach.

The existence of a self-preserving distribution for coagulation in the continuum regime is shown in [34]. A shape-invariant distribution (in particular the logarithmic volume distribution) is also found for the free molecular regime [35,36]. Long time simulations of particles undergoing coagulation and sintering (for particular coagulation kernels), reveal the existence of a self-preserving limit, where the particle distribution remains invariant under a particular scaling transformation [37,38,6]. Thus, dynamic renormalization and fixed point algorithms (e.g. Newton – GMRES [39]) can be applied to the results of short bursts of appropriately initialized CNMC simulations to locate coarse self-similar solutions and the corresponding exponents. Such an approach has been successful in a variety of equation-free applications [40–42]; it would be natural to explore its use in the context of particulate processes for which the final distribution shapes and similarity exponents are not known.

We reiterate that the approach described here can, in principle, be wrapped around different types of inner, fine-scale, particle simulators (e.g. molecular dynamics, dissipative particle dynamics or Brownian dynamics simulators). It can be used in cases where more physical processes than only coagulation and sintering occur (e.g. when particle fragmentation, or even particle surface reactions are incorporated in the fine-scale code). One of the most important limitations of the approach is the need to know *at what level* one can write a successful closed model – alternatively, what the right coarse variables are. While for many problems these variables are known from long modeling experience (e.g. leading moments here), one can envision the use of data-mining tools, such as Isomap, or diffusion maps [44,43] for the data-based detection of good coarse observables in new problems, in which intuition or extensive experience is lacking.

Acknowledgments

We thank Prof. R. Dennis Vigil for his helpful suggestions to this work and for sending us one of his codes for our reference. The research of ROF was supported by NSF (CBET-0730250 and CBET-0403864). I.G.K., Y.Z. and M.E.K. also gratefully acknowledge support by the National Science Foundation as well as the US DOE.

Appendix A

An alternative approach for the construction of particle distribution realizations, which are consistent with a given coarse-grained description (values of a finite number of distribution moments), is based on the application of the maximum entropy method (*maxent*) [28,29]. *Maxent* generates the least-biased approximation of a function, for which only limited information is available. When this information is in the form of values of a finite number of moments, one seeks the maximization of the Shannon entropy functional [45], under the constraint that the values of the first N moments are the ones prescribed. Such a univariate distribution, $n(u)$, will optimize the Lagrangian functional:

$$L(n^{lift}, \underline{\lambda}) = -\int n^{lift}(v)\ln n^{lift}(v)\,\mathrm{d}v + \sum_{i=1}^{N}\lambda_i\left(\int v^{i-1}n^{lift}(v)\,\mathrm{d}v - M_{i-1}\right). \tag{A-1}$$

Here, $n^{lift}(v)$ is the approximating number density of particles as a function of the particle volume, v; M_i is the prescribed value of the ith moment and $\underline{\lambda}$ is the vector of the associated Lagrange multipliers. According to the maximum entropy method, $n^{lift}(v)$ is:

$$n^{lift}(v) = \exp\left(\sum_{i=1}^{N}(\lambda_i v^{i-1}) - 1\right). \tag{A-2}$$

Given the values of a number of moments of a particle distribution, lifting for univariate QMOM–MC computations can be implemented through the following steps:

(a) Compute the Lagrange multipliers which maximize the Lagrangian functional (A-1). The computation involves discretization of the integral forms, using a quadrature formula (e.g. Gauss–Legendre). The Shannon entropy functional can, for example, be approximated by:

$$S(v) = -\int n^{lift}(v)\ln n^{lift}(v)\,\mathrm{d}v \approx -\sum_{i=1}^{n} w_i n^{lift}(v_i)\ln n^{lift}(v_i), \tag{A-3}$$

where w_i and v_i are the weights and abscissas of the applied quadrature scheme, respectively. The Lagrange multipliers are evaluated from the solution of:

$$R_k \equiv \sum_{i=1}^{n} w_i v_i^{k-1}\exp\left(\sum_{j=1}^{N}\left(\lambda_j v_i^{j-1}\right) - 1\right) - M_{k-1} = 0, \quad k = 1,2,\ldots,N. \tag{A-4}$$

The set of nonlinear equations (A-4) can be solved with the Newton–Raphson method, where at each iteration an update, $\delta\underline{\lambda}$, of the Lagrange multipliers is calculated through the solution of the linear system:

$$\underline{\underline{H}}\delta\underline{\lambda} = -\underline{R}, \tag{A-5}$$

with:

$$H_{kj} = \frac{\partial R_k}{\partial \lambda_j} = \sum_{i=1}^{n} w_i v_i^{j-1} v_i^{k-1}\exp\left(\sum_{j=1}^{N}\left(\lambda_j v_i^{j-1}\right) - 1\right), \quad k,\ j = 1,2,\ldots,N. \tag{A-6}$$

The sought multipliers $\underline{\lambda}$ are updated through the relation $\underline{\lambda}^{(m+1)} = \underline{\lambda}^{(m)} + \delta\underline{\lambda}$, where m denotes the iteration step. Upon convergence, the computed Lagrange multipliers are used in (A-2) to construct the approximating density function $n^{lift}(v_i)$. At this point we have to stress that the estimation of the *maxent* density becomes sensitive to the choice of initial guesses in the iterative Newton–Raphson procedure as the number of moment constraints rises, partially because the Hessian matrix (A-6) approaches singularity as its dimension increases. In this case alternative techniques may be applied, based on a sequential computation of the Lagrange multipliers. For further reading see [46,29].

(b) We compute the corresponding cumulative distribution function, $F(v_j)$, according to:

$$F(v_j) = \frac{\sum_{i=1}^{j} w_i n^{lift}(v_i)}{\sum_{i=1}^{n} w_i n^{lift}(v_i)} \tag{A-7}$$

and generate a consistent microscopic particle distribution. For each of the N_p particles, a random number p is drawn from the uniform distribution $U(0,1)$. Then, the particle k $(1 \leqslant k \leqslant N_p)$ is assigned a volume, v_j, if $F(v_{j-1}) < p < F(v_j)$ (we define: $F(v_0) = 0$). This procedure leads to the generation of a distribution which is consistent with the given coarse-grained description (values of the first few moments).

References

[1] W. Koch, S.K. Friedlander, The effect of particle coalescence on the surface area of a coagulating aerosol, J. Colloid Interf. Sci. 140 (1990) 419–427.
[2] T. Matsoukas, S.K. Friedlander, Dynamics of aerosol agglomerate formation, J. Colloid Interf. Sci. 146 (1991) 495–506.
[3] M. Smoluchowski, Drei Vorträge über Diffusion, Brownsche Molekularbewegung und Koagulation von Kolloidteilchen, Physica Z 17 (1916) 557–571. and 585–599.
[4] D. Ramkrishna, Population Balances: Theory and Applications to Particulate Systems in Engineering, Academic Press, New York, 2000.
[5] R. McGraw, Description of aerosol dynamics by the quadrature method of moments, Aerosol Sci. Technol. 27 (1997) 255–265.
[6] D.L. Wright, R. McGraw, D.E. Rosner, Bivariate extension of the quadrature method of moments for modeling simultaneous coagulation and sintering of particle populations, J. Colloid Interf. Sci. 236 (2001) 242–251.
[7] D.L. Marchisio, R.D. Vigil, R.O. Fox, Quadrature method of moments for aggregation-breakage processes, J. Colloid Interf. Sci. 258 (2003) 322–334.
[8] D.L. Marchisio, R.O. Fox, Solution of population balance equations using the direct quadrature method of moments, J. Aerosol Sci. 36 (2005) 43–73.
[9] R.O. Fox, Bivariate direct quadrature method of moments for coagulation and sintering of particle populations, J. Aerosol Sci. 37 (2006) 1562–1580.
[10] L.A. Spielman, O. Levenspiel, A Monte-Carlo treatment for reacting and coalescing dispersed phases systems, Chem. Eng. Sci. 20 (1965) 247–254.
[11] P. Meakin, The growth of fractal aggregates, in: R. Pynn, T. Riste (Eds.), Time-Dependent Effects in Disordered Materials, Plenum Press, New York, 1987, pp. 45–70.
[12] K. Liffman, A direct simulation Monte-Carlo method for cluster coagulation, J. Comput. Phys. 100 (1992) 116–127.
[13] M. Smith, T. Matsoukas, Constant-number Monte Carlo simulation of population balances, Chem. Eng. Sci. 53 (1998) 1777–1786.
[14] K. Theodoropoulos, Y.-H. Qian, I.G. Kevrekidis, Coarse stability and bifurcation analysis using time-steppers: a reaction–diffusion example, Proc. Natl. Acad. Sci. 97 (2000) 9840–9843.
[15] C.W. Gear, I.G. Kevrekidis, C. Theodoropoulos, Coarse integration/bifurcation analysis via microscopic simulators: micro-Galerkin methods, Comput. Chem. Eng. 26 (2002) 941–963.
[16] I.G. Kevrekidis, C.W. Gear, J.M. Hyman, P.G. Kevrekidis, O. Runborg, C. Theodoropoulos, Equation-free coarse-grained multiscale computation: enabling microscopic simulators to perform system-level tasks, Commun. Math. Sci. 1 (2003) 715–762.
[17] I.G. Kevrekidis, C.W. Gear, G. Hummer, Equation-free: the computer-aided analysis of complex multiscale systems, AIChE J. 50 (2004) 1346–1355.
[18] Y. Xiong, S.E. Pratsinis, Formation of agglomerate particles by coagulation and sintering—Part I. A two-dimensional solution of the population balance equation, J. Aerosol Sci. 24 (1993) 283–300.
[19] A.D. Randolph, M.A. Larson, Theory of Particulate Processes, second ed., Academic Press, New York, 1988.
[20] J.A. Shohat, J.D. Tamarkin, The Problem of Moments, Mathematical Surveys, second ed., vol. 1, American Mathematical Society, Providence, RI, 1950.
[21] R.G. Gordon, Error bounds in equilibrium statistical mechanics, J. Math. Phys. 9 (1968) 655–663.
[22] W.H. Press, S.A. Teukolsky, W.T. Vetterling, B.P. Flannery, Numerical Recipes in C, second ed., Cambridge University Press, New York, 1992.
[23] H. Rutishauser, Der Quotienten-Differenzen Algorithmus, Birkhäuser-Verlag, Basel, 1957.
[24] C.W. Gear, Projective integration methods for distributions, NEC Technical Report, 2001-130, 2001.
[25] R. Rico-Martínez, C.W. Gear, I.G. Kevrekidis, Coarse projective kMC integration: forward/reverse initial and boundary value problems, J. Comput. Phys. 196 (2004) 474–489.
[26] M.E. Kavousanakis, R. Erban, A.G. Boudouvis, C.W. Gear, I.G. Kevrekidis, Projective and coarse projective integration for problems with continuous symmetries, J. Comput. Phys. 225 (2007) 382–407.
[27] J.C. Wheeler, Modified moments and Gaussian quadratures, Rocky Mt. J. Math. 4 (1974) 287–296.
[28] L.R. Mead, N. Papanicolaou, Maximum entropy in the problem of moments, J. Math. Phys. 25 (1984) 2404–2417.
[29] K. Bandyopadhyay, A.K. Bhattacharya, P. Biswas, D.A. Drabold, Maximum entropy and the problem of moments: a stable algorithm, Phys. Rev. E 71 (2005) 057701–057704.
[30] R.D. Mountain, G.W. Mulholland, H. Baum, Simulation of aerosol agglomeration in the free molecular and continuum flow regimes, J. Colloid Interf. Sci. 114 (1986) 67–81.
[31] D.R. Kincaid, E.W. Cheney, Numerical Analysis: Mathematics of scientific computing, second ed., Brooks/Cole Publishing Company, New York, 1996.
[32] R.S. Anderssen, P. Bloomfield, Numerical differentiation procedures for non-exact data, Numer. Math. 22 (1974) 157–182.
[33] S. Vemury, K.A. Kusters, S.E. Pratsinis, Time-lag for attainment of the self-preserving particle size distribution by coagulation, J. Colloid Interf. Sci. 165 (1994) 53–59.
[34] S.K. Friedlander, C.S. Wang, The self-preserving particle size distribution for coagulation by Brownian motion, J. Colloid Interf. Sci. 22 (1966) 126–132.
[35] F.S. Lai, S.K. Friedlander, J. Pich, G.M. Hidy, The self-preserving particle size distribution for Brownian coagulation in the free-molecule regime, J. Colloid Interf. Sci. 39 (1972) 395–405.
[36] K.E.J. Lehtinen, M.R. Zachariah, Self-preserving theory for the volume distribution of particles undergoing Brownian coagulation, J. Colloid Interf. Sci. 242 (2001) 314–318.
[37] P. Tandon, D.E. Rosner, Monte-Carlo simulation of particle aggregation and simultaneous restructuring, J. Colloid Interf. Sci. 213 (1999) 273–286.
[38] D.E. Rosner, S. Yu, MC simulation of aerosol aggregation and simultaneous spheroidization, AIChE J. 47 (2001) 545–561.
[39] C.T. Kelley, Iterative Methods for Linear and Nonlinear Equations, SIAM, Philadelphia, 1995.

[40] L. Chen, P.G. Debenedetti, C.W. Gear, I.G. Kevrekidis, From molecular dynamics to coarse self-similar solutions: a simple example using equation-free computation, J. Non-Newtonian Fluid Mech. 120 (2004) 215–223.
[41] A. Szell, D. Merritt, I.G. Kevrekidis, Core collapse via coarse dynamic renormalization, Phys. Rev. Lett. 95 (2005) 081102–081104.
[42] D.A. Kessler, I.G. Kevrekidis, L. Chen, Equation-free dynamic renormalization of a Kardar–Parisi–Zhang type equation, Phys. Rev. E 73 (2006) 036703–036706.
[43] B. Nadler, S. Lafon, R.R. Coifman, I.G. Kevrekidis, Diffusion maps, spectral clustering and reaction coordinates of dynamical systems, Appl. Comput. Harm. Anal. 21 (2006) 113–127.
[44] J.B. Tenenbaum, V. de Silva, J.C. Langford, A global geometric framework for nonlinear dimensionality reduction, Science 290 (2000) 2319–2323.
[45] C.E. Shannon, A mathematical theory of communication, Bell Syst. Tech. J. 27 (1948) 379–423.
[46] Ximing Wu, Calculation of maximum entropy densities with application to income distribution, J. Econom. 115 (2003) 347–354.